NOTES

Supercritical flow at an abrupt drop: flow patterns and aeration

H. Chanson and L. Toombes

Abstract: Stepped waterways and cascades are common features of storm waterways, at dam outlets, and in water treatment plants. At an abrupt drop, open channel flows are characterized by the presence of shock waves and a substantial flow aeration. There is, however, little information on the basic flow characteristics. The study presents new experimental data obtained in a 0.5-m-wide stepped flume with an unventilated nappe. The investigations describe the three-dimensional flow patterns, including shock waves, standing waves, and spray, downstream of the nappe impact. The characteristics of the flow patterns are similar to those observed with abrupt expansion supercritical flows. Downstream of the drop brink, substantial aeration takes place along the nappe interfaces and the flow downstream of the impact is deaerated.

Key words: abrupt drop, supercritical flow, shock waves, flow patterns, cascade.

Résumé : Des canaux en escalier et des cascades sont des composantes communes de canaux pluviaux, de déversoirs de barrages et d'instalations de traitement des eaux. Sujets à une chute raide, les débits libres sont caractérisés par la présence d'ondes de choc et d'une aération importante. Il y a cependant très peu d'informations au sujet des caractéristiques de base du débit. Cet étude présente de nouveaux résultats expérimentaux obtenus à partir d'un canal en escalier de 0,5 m de largeur avec nappe non-ventilée. L'étude décrit les caractéristiques à trois dimensions du débits, y compris les ondes de choc, les ondes stationnaires et la poussière d'eau en aval de la nappe d'impact. Les caractéristiques du débit approchent les observations de débits supercritiques sujets à une expansion raide. A l'interface de la nappe, en aval de la cime des chutes, l'aération s'avère importante alors que le relachement des gaz se fait en aval de l'impact.

Mots clés : chute raide, débit supercritique, ondes de choc, caracteristiques de débit, cascade.

[Traduit par la Rédaction]

1. Introduction

In storm waterways, at dam outlets, and in water treatment plants, it is common to design drops, stepped waterways, and cascades. At each drop, the supercritical flow takes off as a free-falling nappe before impacting onto the downstream invert. Substantial flow aeration, referred to as "white water," is observed and there is little information on the air–water flow characteristics.

It is the purpose of this study to present new information on the supercritical flow at an abrupt drop and the free-surface aeration. The study is based on new experimental data obtained in a large channel at the University of Queensland. The results are compared with supercritical flows at an abrupt expansion and with prototype observations at the Gold Creek dam cascade, Australia.

Received July 31, 1997.
Revised manuscript accepted February 18, 1998.

H. Chanson and L. Toombes. Department of Civil Engineering, The University of Queensland, Brisbane QLD 4072, Australia.

Written discussion of this note is welcomed and will be received by the Editor until June 30, 1999 (address inside front cover).

2. Experimental apparatus and method

The authors conducted a series of new experiments in a 0.5-m-wide channel (Table 1). The flow is issued from an elliptical convergent and the drop, 0.131 m high, is located 2.4 m downstream of the nozzle. The flume is made of planed wooden boards with equivalent surface roughness height of 1 mm. The channel invert, upstream and downstream of the vertical drop, is flat and horizontal (Fig. 1). An overfall is located 2.4 m downstream of the drop and prevents any form of backwater effect.

Water is supplied by a pump, with a variable-speed electronic controller (Taian™ T-verter K1-420-M3 adjustable frequency AC motor drive), enabling an accurate discharge adjustment in a closed-circuit system. Flow to the flume is fed through a smooth convergent nozzle, 1.7 m long, and the nozzle exit is 30 mm high and 0.5 m wide. The observed contraction ratio is unity, i.e., flow depth at the channel intake d_0 = 30 mm for all experiments. Earlier experiments

Table 1. Experimental flow conditions.

q_w (m²/s)	V_o (m/s)	ΔP (Pa)	Comments
0.038	1.27	150	Supercritical flow upstream and downstream of the drop
0.080	2.7	138	Supercritical flow upstream and downsream of the drop
0.130	4.3	31.3	Supercritical flow upstream and downstream of the drop
0.150	5.0	32.8	Supercritical flow upstream and downstream of the drop
0.163	5.4	—	Supercritical flow upstream and downstream of the drop; loud noise generated by air cavity at first drop

Notes: Approach flow depth d_o = 0.03 m; step height h = 0.131 m (horizontal steps); channel width W = 0.5 m.

(Chanson 1995) showed that the flow at the nozzle is two dimensional.

The water discharge is measured with a site-calibrated Dall™ tube flowmeter. The accuracy of the discharge measurement is about 2%. In the absence of free-surface aeration, flow depths were measured with a point gauge. Air concentration measurements were performed using a single-tip conductivity probe developed at the University of Queensland (Chanson 1995). The probe consists of an internal concentric platinum electrode of diameter 0.35 mm and an external stainless steel electrode of diameter 1.42 mm. The probe is aligned in the direction of flow and excited by an air bubble detector (AS25240). This electronic system was designed with a response time of less than 10 μs and calibrated with a square wave generator.

The translation of the probe in the direction normal to the channel bottom was controlled by a fine adjustment travelling mechanism connected to a Mitutoyo™ digimatic scale unit (Ref. No. 572-503). The error on the vertical position of the probe was less than 0.025 mm. The system consisting of probe and travelling mechanism was mounted on a trolley system. The accuracy on the longitudinal probe position was estimated to $\Delta x < \pm 1$ cm. The accuracy on the transverse position of the probe was estimated to $\Delta z < \pm 1$ mm.

Nappe cavity subpressures were recorded with a projection manometer (TEM Engineering™, Ref. M939). The accuracy of the manometer is about ±1 Pa. In addition, high-speed photographs were taken to analyse the flow patterns. Further details of the instrumentation and the full set of experimental data are reported in Chanson and Toombes (1997).

3. Flow patterns

3.1. Presentation

With the abrupt-drop geometry, experimental observations indicate that the water flows as a supercritical flow upstream and downstream of the abrupt drop for all the investigated flow conditions (Table 1). At the end of the drop, the flow becomes a free-falling jet and the air cavity beneath the nappe was well established (Fig. 1). Note that the air cavity was normally not ventilated. Nappe cavity subpressures are reported in Table 1. For one particular discharge (i.e., water discharge per unit width $q_w \approx 0.163$ m²/s), loud noise occurred, generated by inadequate nappe ventilation leading to fluttering instabilities. The noise could be stopped by ventilating the air cavity. Observations showed that the approach flow and the free-falling nappe were basically two dimensional. Downstream of the nappe impact, the flow became three dimensional and white water was observed (Fig. 2).

3.2. Basic flow patterns

For all flow rates investigated, the jet impact induced significant water splashing and jet deflection, followed by the propagation of oblique shock waves intersecting farther downstream on the channel centreline (Figs. 1, 2). The nappe impact on the horizontal step is characterized by a change of flow direction in the vertical streamwise plane and by some flow deceleration caused by energy dissipation at drop impact. The change of streamline direction in the supercritical flow induces the propagation of shock waves.

For $d_c/h < 0.84$, where d_c is the critical flow depth and h is the step height, the shock waves are basically straight and intersect upstream of the downstream overfall (Figs. 1*a*, 2*a*). For $d_c/h > 0.84$, the cross waves are not straight. Each shock wave exhibits a broken line (Figs. 1*c*, 2*d*). At the sidewall, the angle between the shock wave and the flow direction appears to be greater than the angle observed farther downstream. The decrease in shock-wave angle seems to correspond to the location where the spray reattaches to the main stream (Fig. 1*c*). Standing waves are also observed at the impact of the nappe along the sidewalls (Fig. 2*b*). Note that the location of maximum height of the wall standing waves does not coincide exactly with the start of the cross waves.

For $d_c/h = 0.84$, the shock waves developing downstream of the nappe impact intersect at the brink of the downstream overfall (i.e., edge of second overfall). Immediately downstream of the shock-wave intersection, a "rooster tail" wave takes place on the centreline of the second free-falling nappe, "riding" over the upper nappe (Figs. 1*b*, 2*c*). For $d_c/h > 0.84$, the shock waves downstream of the drop intersect downstream of the brink of the overfall (Fig. 1*c*).

3.3. Discussion

Significant jet deflection, shock waves, and standing waves are observed downstream of the drop. Interestingly two types of shock-wave intersection are observed downstream of the drop. At low flow rates (i.e., $d_c/h < 0.66$), the cross waves intersect without significant interference: this type is typical in nonaerated supercritical flows. For $d_c/h > 0.66$, the free surface behind the shock waves is characterized by turbulent wavelets and the free-surface looks rougher downstream of the cross waves.

4. Shock-wave characteristics

The characteristics of the standing waves and of the cross waves were recorded and the main results are presented in Figs. 3–6.

Fig. 1. Sketches of typical flow patterns on the first steps. Flow pattern for (*a*) $d_c/h < 0.84$, (*b*) $d_c/h = 0.84$, and (*c*) $d_c/h > 0.84$.

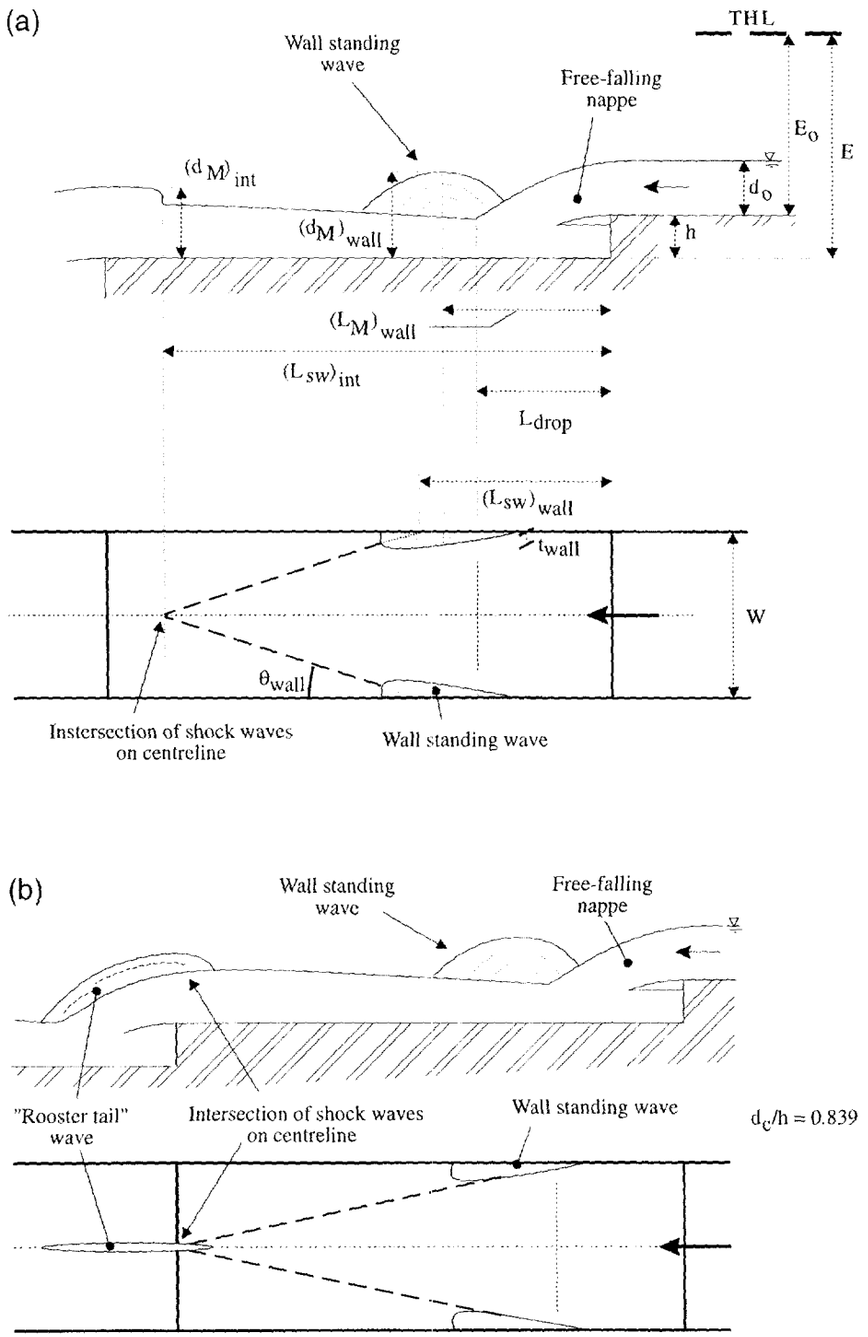

Figure 3 presents the dimensionless drop length L_{drop}/W, the location of the maximum standing wave free-surface elevation $(L_M)_{wall}/W$, the position of the start of shock waves at the sidewall $(L_{sw})_{wall}/W$, and the position of the intersection of shock waves $(L_{sw})_{int}/W$, where W is the downstream channel width. The data are plotted as functions of the downstream ideal flow Froude number Fr defined in Appendix 2.

Figure 3 indicates a consistent increase in dimensionless drop length and locations of the standing wave and cross waves with increasing Froude number. The drop-length data compare favourably with experimental data by Dominguez (1974, p. 390, Fig. 196). They are best correlated by the following (data from the present study):

$$[1] \qquad \frac{L_{drop}}{W} = 0.22(\mathrm{Fr} - 3.15)$$

$$[2] \qquad \frac{(L_M)_{wall}}{W} = 2.98\frac{\mathrm{Fr} + 3.93}{\mathrm{Fr}^2 + 37.7}(\mathrm{Fr} - 3.93)$$

Fig. 1 (*concluded*).

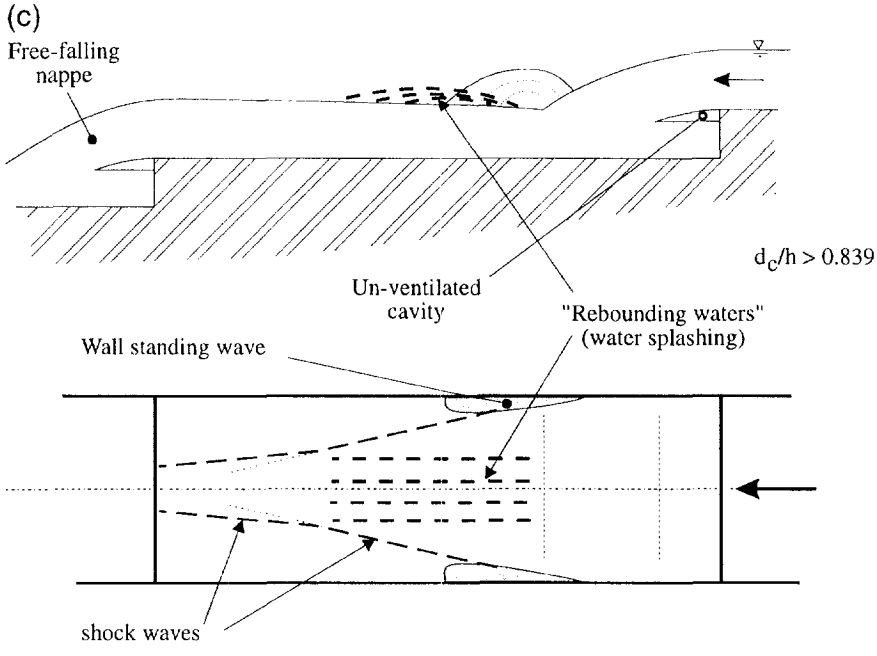

$$[3] \quad \frac{(L_{SW})_{wall}}{W} = 0.44(Fr - 4.51)$$

$$[4] \quad \frac{(L_{SW})_{int}}{W} = 0.70(Fr - 1.78)$$

For the design of chutes and sewers, the wave heights are determining parameters. In Fig. 4 the dimensionless wave heights at the wall and at the shock-wave intersection are plotted as functions of the downstream Froude number, where $fE = E_o + h$ is the upstream total head (where E and E_o are the mean and upstream specific energy, respectively), taking the downstream channel bed as datum. The data are compared with reanalysed data of supercritical flows at channel expansions (Table 2). Figure 4 shows a close agreement between the wave heights at an abrupt drop and at an abrupt expansion. At an abrupt drop, the impinging nappe experiences a change in momentum direction and some flow deceleration caused by energy dissipation. The flow pattern is somewhat similar to that of a supercritical flow at a sudden channel expansion. That is, the flow is subjected to a rapid change of streamline direction and a sudden deceleration with propagation of oblique shock waves and flow deflection along the sidewall. The data are best correlated by

$$[5] \quad \frac{(d_M)_{wall}}{E} = \frac{5.43}{Fr^{2.0}}$$

(data from the present study and Hager and Mazumder 1992)

$$[6] \quad \frac{(d_M)_{int}}{E} = 5.3 \times 0.77$$

(data from the present study, Hager and Mazumder 1992, and Mazumder and Hager 1993), where $(d_M)_{wall}$ is the maximum height of the sidewall standing wave, and $(d_M)_{int}$ is the maximum height at the shock-wave intersection on the channel centreline.

The wave heights are a form of potential energy which account for 5–20% of the total energy of the flow. Note that the standing-wave heights are consistently higher at the wall than on the centreline.

Figure 5 presents the dimensionless standing-wave thickness (at maximum wave height) t_{wall}/E versus the downstream Froude number Fr (eq. [7]). The data are compared with reanalysed data obtained at a 30° channel junction (Table 2). Interestingly, the standing-wall thickness is of the same order of magnitude as the sidewall wave height (Figs. 4, 5). Note that the standing wave has a "drop" shape (Fig. 1) and its maximum thickness is located at its downstream end. Overall the data are best fitted by the following (data from the present study):

$$[7] \quad \frac{t_{wall}}{E} = 0.0063(7.15E + 5)^{1/(Fr-1)}$$

The shock-wave angle data are shown in Fig. 6 and compared with reanalysed data at channel expansions. In Fig. 6, the authors' data are presented in two series: the angle measured at the wall and the angle measured near the downstream overfall after the reattachment of spray for the largest discharges (Fig. 1*c*).

For flows with a significant spray development, visual observations suggest that the rebounding waters reattach to the main stream with impact velocities larger than those of the mean flow. If this hypothesis is verified, the flow immediately downstream of the impact would be slower than the spray, leading to a wider shock-wave angle at the wall, as suggested by Fig. 6. Overall the data downstream of the spray reattachment show a decrease of shock-wave angle with increasing Froude number: the result is consistent with most observations in supercritical flows. Further, the present series of data is in close agreement with the shock-wave angle at an abrupt channel expansion. The shock-wave angle

Fig. 2. Photographs of oblique shock waves and sidewall standing waves. (*a*) Oblique shock waves (arrow) downstream of the drop (d_c/h = 0.87). Flow from bottom to top. High-speed photographs taken at night (67 μs flash speed). (*b*) Sidewall standing waves downstream of the drop (d_c/h = 0.77). Flow from left to right. (*c*) Oblique shock waves downstream of the drop with rooster tail wave developing downstream of the shock-wave intersection and onto the second overfall (d_c/h = 0.91). Flow from bottom to top. (*d*) Oblique shock waves with a broken line shape near the downstream overfall (d_c/h = 0.92). Flow from bottom to top. High-speed photographs taken at night (67 μs flash speed).

Fig. 3. Dimensionless lengths (L) at the first drop as functions of the downstream Froude number (ideal flow): drop length L_{drop}/W, position of the maximum standing wave height $(L_M)_{wall}/W$, position of the start of shock waves at the wall $(L_M)_{wall}/W$, and position of the intersection of shock waves $(L_{sw})_{int}/W$. Data are from the present study except as indicated.

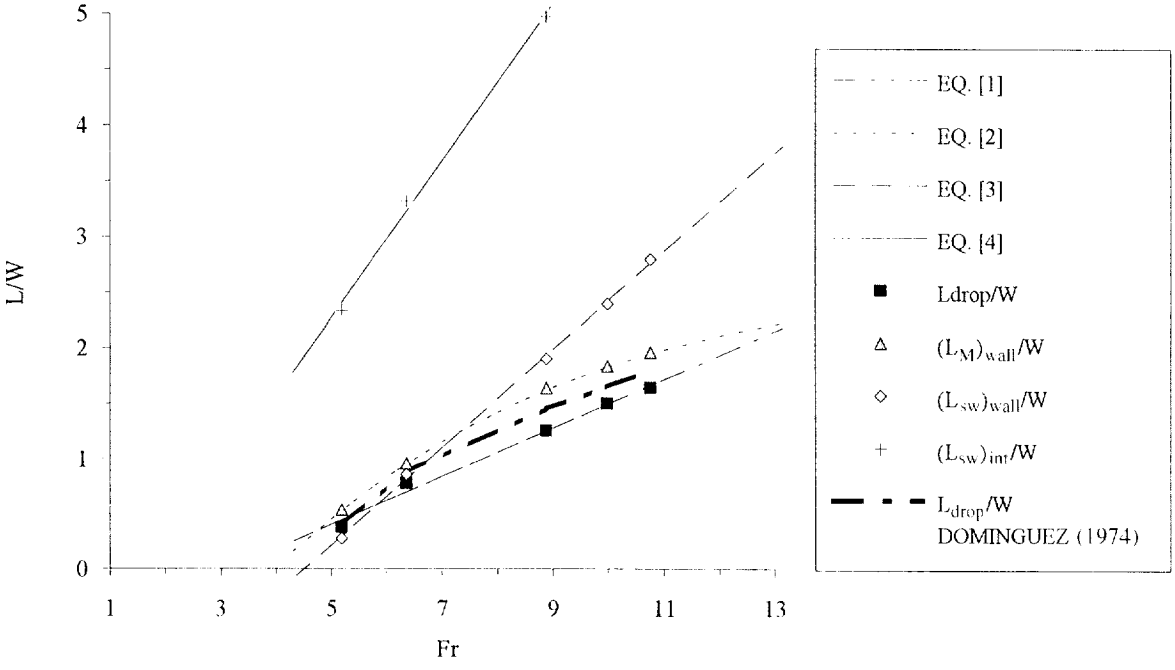

Fig. 4. Dimensionless maximum free-surface heights at the wall $(d_M)_{wall}/W$ and at the intersection of shock waves on the channel centreline $(d_M)_{int}/E$ as functions of the downstream Froude number (ideal flow) (Table 3).

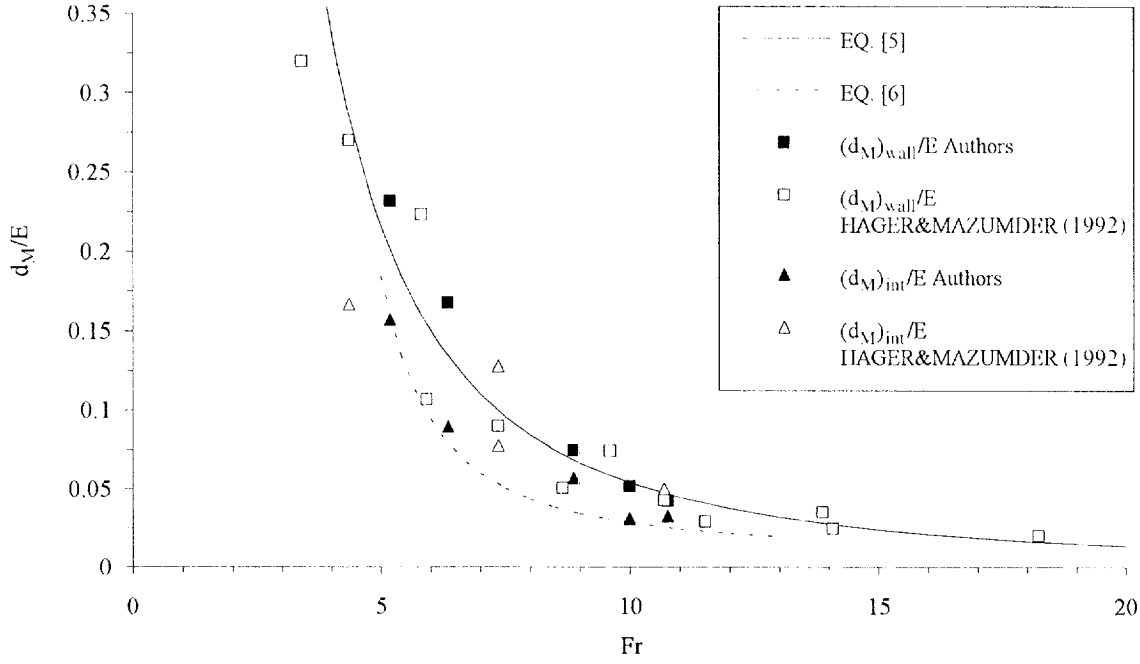

data θ, in degrees, are best correlated by the following (data from the present study):

$$[8] \qquad \theta = \frac{645}{(\mathrm{Fr}-1)^{1.1}}$$

5. Nappe flow and air entrainment

For one flow rate, $d_c/h = 1.0$, air concentration distributions were measured in the nappe and downstream of the nappe on the channel centreline and next to the sidewall. Figure 7*a* presents the centreline data, and Fig. 7*b* shows the

Fig. 5. Dimensionless thickness of the sidewall standing wave at the maximum free-surface height at the wall t_{wall}/E as a function of the downstream Froude number (ideal flow) (Table 3).

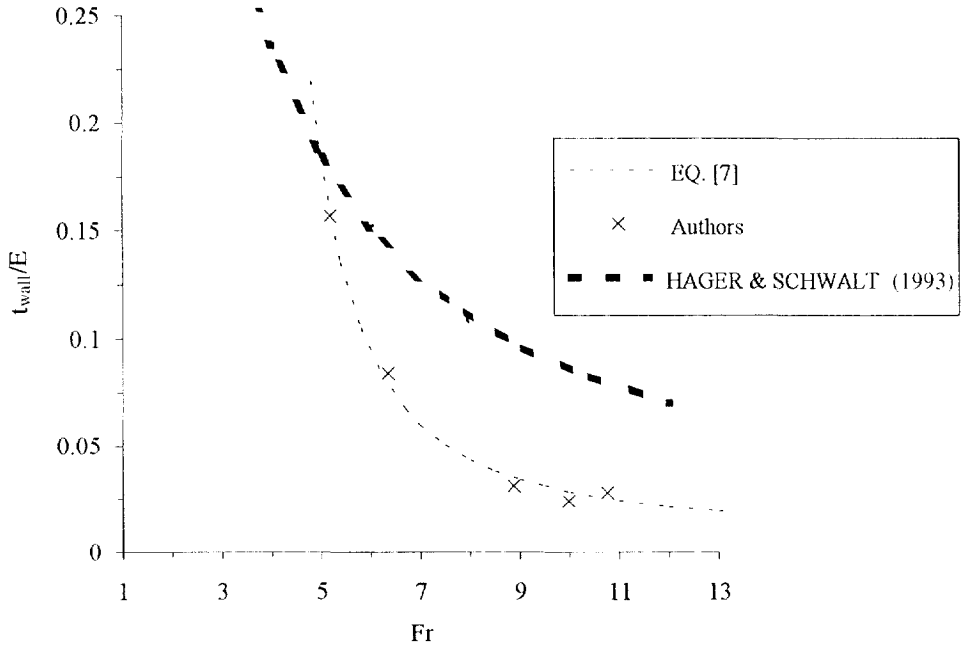

Fig. 6. Shock-wave angle with sidewall θ_{wall} as a function of the downstream Froude number (ideal flow) (Table 3). d/s, downstream.

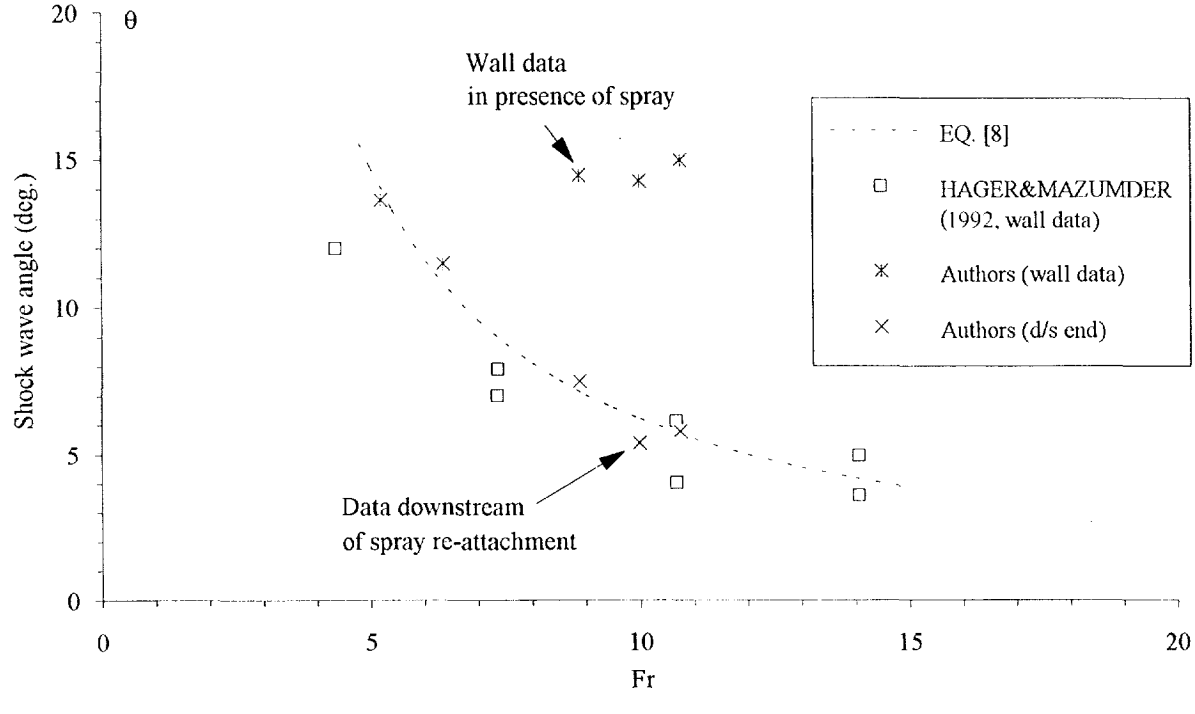

air concentration profiles 1.7 mm from the sidewall. The unventilated air cavity, the impact point, and the spray region are indicated. In each figure, dotted lines give the cross-section locations used as the local zero air content.

The air concentration data highlight a large air cavity as the main feature of the air–water flow. Nappe subpressure measurements (Table 1) indicate that the cavity pressure is nearly atmospheric. The nappe aeration occurs along the sidewall and possibly by free-surface aeration across the upper nappe. The sidewall standing waves and the spray are clearly observed in Figs. 7*b* and 7*a*, respectively. The spray region is characterized by a large amount of flow aeration, with a multitude of water droplets surrounded by air. Downstream of the spray reattachment, a significant axial air de-aeration takes place. At the end of the invert, the mean air concentration C_{mean} is still about 0.19.

Table 2. Analysis and reanalysis of experimental data of shock waves in supercritical flows.

Type of flow	Reference	Flow conditions	Remarks
Abrupt drop	Present study	Fr_o = 2.3–10, d_o = 0.03 m, W = 0.5 m	Laboratory experiments in a rectangular channel
Abrupt channel expansion	Hager and Mazumder (1992)	Fr_o = 3.4–18.2, d_o = 0.024–0.096 m, W_o = 0.25 and 0.5 m, W/W_o = 2, 3, and 5	Laboratory experiments in a horizontal rectangular channel
Channel expansion	Mazumder and Hager (1993)	Modified Rouse type: Fr_o = 8, d_o = 0.048 m, W_o = 0.5 m, W/W_o = 3; reverse Rouse type: Fr_o = 4, d_o = 0.096 m, W_o = 0.5 m, W/W_o = 3	Laboratory experiments in a horizontal rectangular channel
Channel junction	Schwalt and Hager (1993)	Fr_o = 2.5–12, d_o = 0.02–0.10 m, W_o = W = 0.5 m, 30° junction (lateral inflow = outflow)	Laboratory experiments in a horizontal rectangular channel

Notes: Fr_o, inflow Froude number; W_o, inflow channel width; W, downstream channel width.

Fig. 7. Air concentration measurement in supercritical flow at an abrupt drop: (*a*) q_w = 0.15 m²/s, centreline data; and (*b*) q_w = 0.15 m²/s, measurements at 1.7 mm from the sidewall.

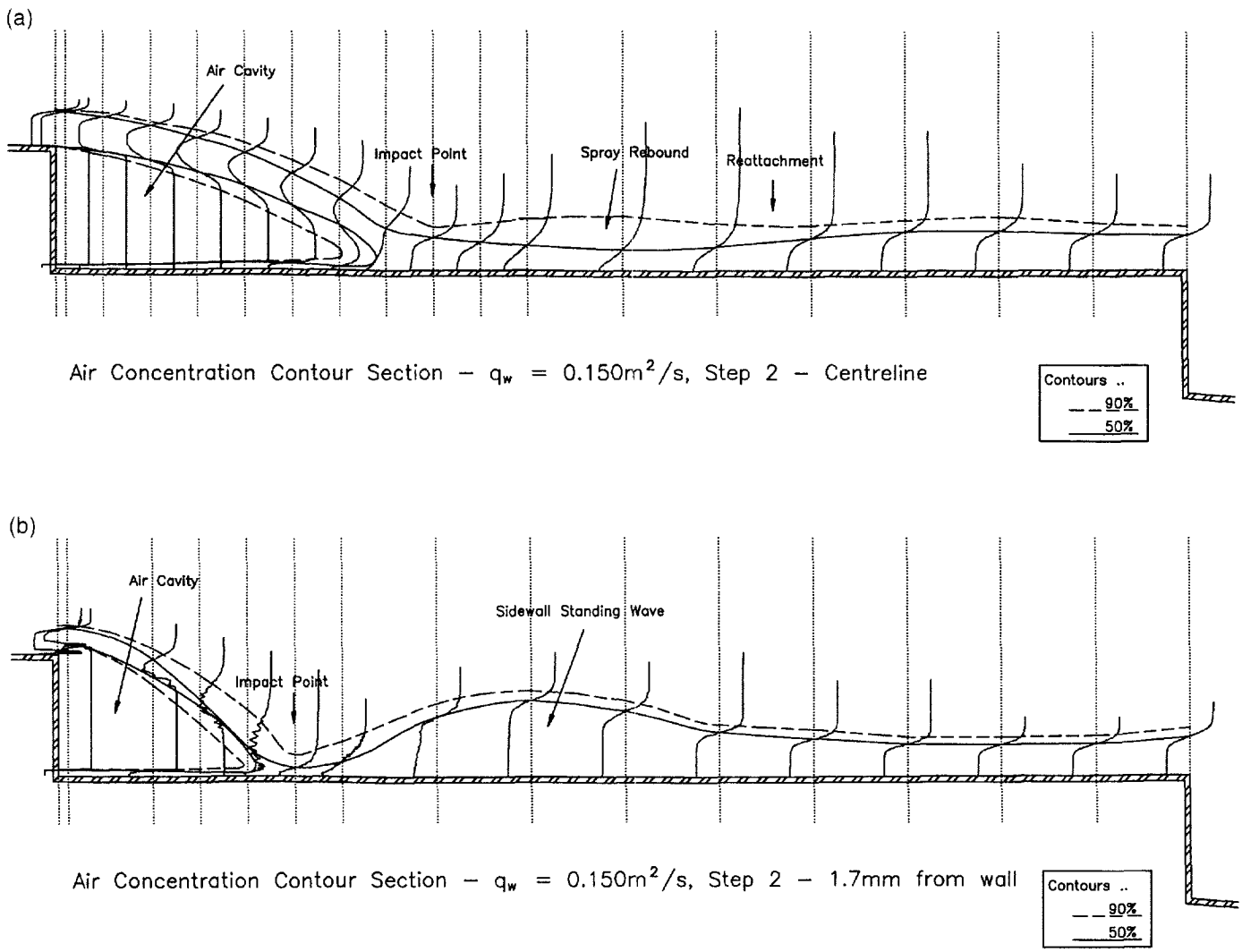

Large amounts of entrained air are observed near the nappe impact, in the spray region, and in the standing waves. Overall the results (Figs. 7*a*, 7*b*) highlight the three-dimensional pattern of the air-entrainment process.

6. Discussion: a prototype experience

A related flow situation was observed at the Gold Creek dam cascade (Chanson and Whitmore 1996) (Fig. 8). The

Fig. 8. Nappe flow above the Gold Creek dam spillway on 2 May 1996 (discharge 27 m^3/s). Spillway characteristics: h = 1.5 m, 20.6° slope, W = 55 m, maximum discharge capacity 280 m^3/s, built in 1890 (unreinforced concrete steps). (*a*) View from the right bank, near the crest. Flow from the left bottom corner to the top right corner. Note the flow past the first small drop (remains of first step) which is not aerated. (*b*) View from downstream. At the end of the chute the flow turns to the right (i.e., left of the photograph) and there is no dissipation structure. Note cross-waves intersecting at the step edges and on the free-falling nappes and the resulting lozenge flow pattern.

(a)

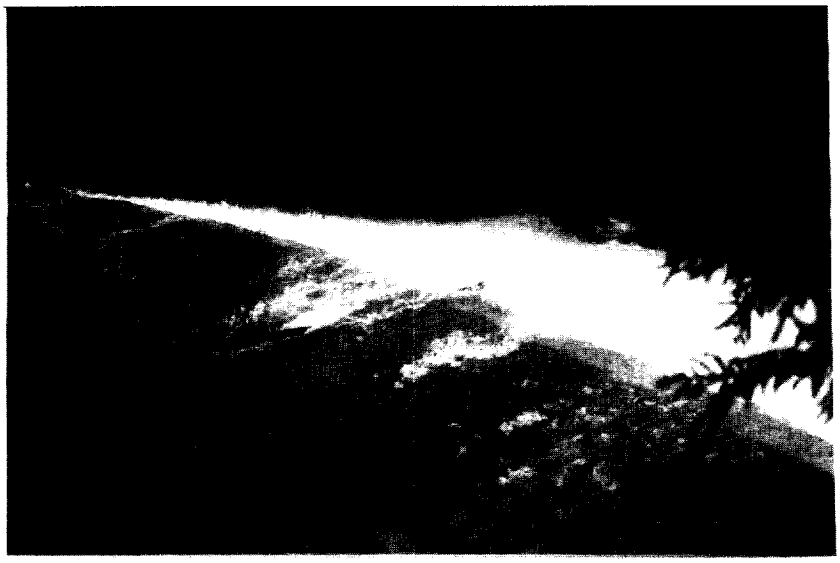

(b)

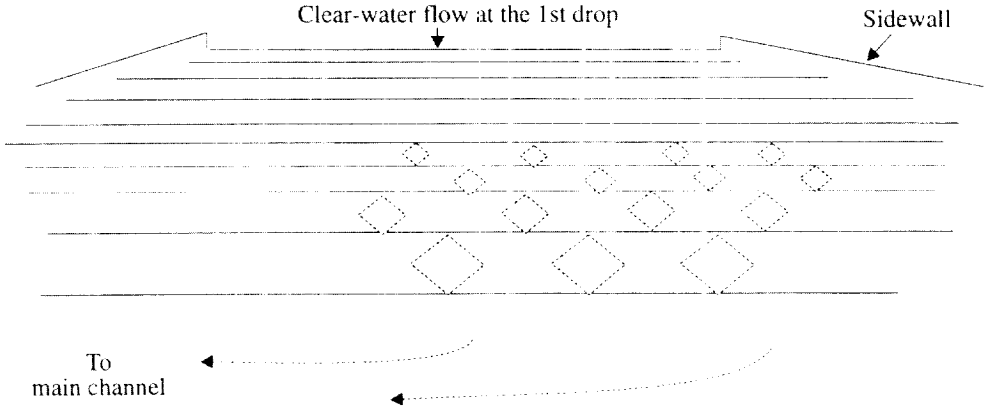

spillway consists of a broad crest, 55 m wide and 61 m long, followed by the remains of the first step (erased in 1975 to enlarge the discharge capacity) and then 11 identical horizontal steps with step height h = 1.5 m and step length l = 4 m. On 2 May 1996 flood waters spilled over the Gold Creek dam spillway following a 200-mm rainfall in 24 h. The discharge was estimated to be 27 m^3/s (q_w = 0.49 m^2/s).[2]

The analysis of colour photographs of the operating spillway indicate that (Fig. 8) (1) the water flows down the chute as a supercritical flow as a succession of free-falling nappes; (2) the flow at the first drop is basically two dimensional and develops to a three-dimensional flow from the second drop (Fig. 8); (3) the flow is highly aerated (i.e., white waters); (4) free-surface aeration take places downstream of the second drop (Fig. 8*a*); and (5) at the end of the chute, the distinction between the air–water flow and the spray is impossible and the water surface has a foam appearance (Fig. 8*b*).

Further, Fig. 8*b* shows free-surface discontinuities which are characteristic of shock-wave intersection next to the step edges. Viewed from downstream (Fig. 8*b*), the free surface of the upper nappes exhibits a series of "lozenges" encompassed in between the shock waves. The angle of the shock waves with the flow direction is about 20–30° at the downstream end of the spillway. For such shock wave angles, eq. [8] would predict a flow Froude number of about 3–4.

7. Conclusions

Supercritical flow at an abrupt drop is investigated experimentally. The study has highlighted several points:

(1) The flow is basically two-dimensional up to the nappe impact and three-dimensional downstream of the nappe impact, with formation of shock waves, standing waves, and spray.

(2) The characteristics of shock waves and standing waves are related to the downstream Froude number Fr, and similarity with abrupt expansion supercritical flows is demonstrated.

(3) The nappe flow is highly aerated along both the upper and lower free surfaces.

(4) The free-surface aeration of the nappe and the rebounding water tend to affect the shock-wave patterns.

(5) A prototype cascade overflow exhibited somewhat similar features, i.e., substantial free-surface aeration and shock-wave development.

The present investigation provides new information on the flow properties of supercritical flows at an abrupt drop. This series of experiments must be extended to predict more accurately the rate of energy dissipation and the complete flow properties of drops and stepped cascades.

Acknowledgements

The authors acknowledge the assistance of Dr. John Macintosh (Water Solutions, Brisbane) and Mr. Richard Tumman (Brookfield, Queensland, Australia) and thank Dr. J.S. Montes (University of Tasmania, Australia) for alerting them to the work of the late Professor Francisco Javier Dominguez. The authors acknowledge the support of the Department of Civil Engineering, the University of Queensland, for providing the experimental facility and the financial support of Australian Research Council (Ref. No. A89331591).

References

Chanson, H. 1995. Air bubble entrainment in free-surface turbulent flows. Experimental investigations. Report CH46/95, Department of Civil Engineering, University of Queensland, Brisbane, Australia.

Chanson, H., and Toombes, L. 1997. Flow aeration at stepped cascades. Research Report No. CE155, Department of Civil Engineering, University of Queensland, Brisbane, Australia.

Chanson, H., and Whitmore, R.L. 1996. Investigation of the Gold Creek Dam Spillway, Australia. Research Report No. CE153, Department of Civil Engineering, University of Queensland, Brisbane, Australia.

Dominguez, F.J. 1974. Hidraulica. [Hydraulics.] 4th ed. Editorial Universitataria, Santiago, Chile. (In Spanish.)

Hager, W.H., and Mazumder, S.K. 1992. Supercritical flow at abrupt expansions. Proceedings of the Institution of Civil Engineers, Water Maritime and Energy, **96**: 153–166.

Mazumder, S.K., and Hager, W.H. 1993. Supercritical expansion flow in Rouse modified and reversed transitions. ASCE Journal of Hydraulic Engineering, **119**(2): 201–219.

Schwalt, M., and Hager, W.H. 1993. Supercritical flow deflection. Proceedings of the 25th IAHR Congress, Tokyo, Japan, Session A, Vol. I, pp. 345–352.

Appendix 1: List of symbols

C: air concentration defined as the volume of air per unit volume of air and water; it is also called void fraction

C_{mean}: mean air concentration defined in terms of 90% air content $\left(C_{mean} = \frac{1}{Y_{90}} \int_0^{Y_{90}} C \, dy \right)$

d: flow depth (m) measured perpendicular to the flow direction

d_c: critical flow depth (m) ($d_c = \sqrt[3]{q_w^2/g}$ in rectangular channel)

$(d_M)_{int}$: maximum height (m) at the shock-wave intersection on the channel centreline

$(d_M)_{wall}$: maximum height (m) of the sidewall standing wave

d_o: flow depth (m) at the channel intake

E: mean specific energy (m)

E_o: upstream specific energy (m)

Fr: Froude number ($Fr = q_w\sqrt{g^2 d^3}$); downstream Froude number

Fr_o inflow Froude number

g: gravity constant (= 9.80 m/s^2 in Brisbane, Australia)

H: mean total head (m)

h: step height (m)

$(L_M)_{wall}$: distance (m) from the vertical face of the step of the maximum sidewall height

L_{drop}: drop length (m) of the free-falling nappe

[2] Estimate deduced from photographs taken before, during, and after the flood event (in April and May 1996).

$(L_{sw})_{int}$: distance (m) from the vertical face of the step of the shock-wave intersection on the channel centreline
$(L_{sw})_{wall}$: distance (m) from the vertical face of the step of the sidewall inception at the sidewall
l: step length (m)
q_w: water discharge per unit width (m^2/s)
t_{wall}: thickness (m) of the sidewall standing wave at the maximum height of the standing wave
V: mean velocity (m/s)
V_o: mean flow velocity (m/s) at channel intake
W: channel width (m)
W_o: inflow channel width (m)
x: horizontal distance along the flow direction (m)
Y_{90}: characteristic air–water flow depth (m) where $C = 0.9$
y: vertical distance (m) measured normal to the channel bottom
Z: altitude (m) or vertical elevation positive upwards
Z_o: bed elevation (m)
z: distance (m) from the sidewall, measured normal to the sidewall (and to the flow direction)
ΔP: nappe cavity subpressure (Pa)
Γ: dimensionless parameter
θ: shock-wave angle with the flow direction
θ_{wall}: shock-wave angle at the sidewall

Subscripts
int: flow conditions at the shock-wave intersection
o: intake flow conditions
wall: flow conditions at the sidewall

Appendix 2: Alternate depths in open channel flow

Considering open channel flow in a rectangular channel, the continuity and the Bernoulli equations state

[A1] $$q_w = Vd$$

[A2] $$H - Z_o = d + \frac{V^2}{2g}$$

where q_w is the discharge per unit width, d is the flow depth, V is the flow velocity, H is the mean total head, Z_o is the bed elevation, and g is the gravity constant. The Bernoulli equation (eq. [A2]) is developed assuming a flat horizontal channel, hydrostatic pressure distribution, and uniform velocity distribution.

For a given specific energy ($E = H - Z_o$) and flow rate q_w, the system of [A1] and [A2] has zero, one, or two solutions depending upon the sign of $\left(H - Z_o - (3/2)\sqrt[3]{q_w^2/g}\right)$. For a positive term, the two possible solutions correspond to a subcritical flow (i.e., Fr $= q_w/\sqrt{gd^3} < 1$) and a supercritical flow.

For a given specific energy and known discharge, the Bernoulli equation is a polynomial equation of degree 3:

[A3] $$\left(\frac{d}{d_c}\right)^3 - \frac{H - Z_o}{d_c}\left(\frac{d}{d_c}\right)^2 + \frac{1}{2} = 0$$

where $d_c = \sqrt[3]{q_w^2/g}$ is the critical flow depth. The three solutions may be expressed in terms of the Froude number:

[A4] $$Fr^{(1)} = \left\{\frac{H - Z_o}{d_c}\left[\frac{1}{3} + \frac{2}{3}\cos\left(\frac{\Gamma}{3}\right)\right]\right\}^{-3/2}$$

subcritical flow

[A5] $$Fr^{(2)} = \left\{\frac{H - Z_o}{d_c}\left[\frac{1}{3} + \frac{2}{3}\cos\left(\frac{\Gamma}{3} + \frac{2\pi}{3}\right)\right]\right\}^{-3/2}$$

complex number

[A6] $$Fr^{(3)} = \left\{\frac{H - Z_o}{d_c}\left[\frac{1}{3} + \frac{2}{3}\cos\left(\frac{\Gamma}{3} + \frac{4\pi}{3}\right)\right]\right\}^{-3/2}$$

supercritical flow

where $\cos\Gamma = 1 - (27/4)[d_c/(H - Z_o)]^3$.

In summary, the downstream ideal flow Froude number in supercritical flow is

[A7] $$Fr = \left\{\frac{E_o + h}{d_c}\left[\frac{1}{3} + \frac{2}{3}\cos\left(\frac{\Gamma}{3} + \frac{4\pi}{3}\right)\right]\right\}^{-3/2}$$

ideal fluid flow

where E_o is the upstream specific energy (i.e., $E_o = d_o + 0.5V_o^2/g$), h is the drop height, and d_c is the critical flow depth for a horizontal channel assuming a hydrostatic pressure distribution.